

Original Article

Design, synthesis, and evaluation of hydroxamic acid-based molecular probes for *in vivo* imaging of histone deacetylase (HDAC) in brain

Changning Wang¹, Thomas E Eessalu², Vanessa N Barth², Charles H Mitch², Florence F Wagner³, Yijia Hong⁴, Ramesh Neelamegam¹, Frederick A Schroeder⁵, Edward B Holson³, Stephen J Haggarty⁵, Jacob M Hooker¹

¹Athinoula A. Martinos Center for Biomedical Imaging, Department of Radiology, Massachusetts General Hospital, Harvard Medical School, Charlestown, MA 02129, USA; ²Eli Lilly & Co., Indianapolis, IN 46285, USA; ³Stanley Center for Psychiatric Research, Broad Institute of Harvard and MIT, 7 Cambridge Center, Cambridge, MA 02142, USA; ⁴Department of Molecular and Cell Biology, University of California, Berkeley, CA 94720, USA; ⁵Chemical Neurobiology Laboratory, Departments of Neurology and Psychiatry, Center for Human Genetic Research, Massachusetts General Hospital, 185 Cambridge Street, Boston, MA 02114, USA

Received August 29, 2013; Accepted October 1, 2013; Epub December 15, 2013; Published January 1, 2014

Abstract: Hydroxamic acid-based histone deacetylase inhibitors (HDACis) are a class of molecules with therapeutic potential currently reflected in the use of suberoylanilide hydroxamic acid (SAHA; Vorinostat) to treat cutaneous T-cell lymphomas (CTCL). HDACis may have utility beyond cancer therapy, as preclinical studies have ascribed HDAC inhibition as beneficial in areas such as heart disease, diabetes, depression, neurodegeneration, and other disorders of the central nervous system (CNS). However, little is known about the pharmacokinetics (PK) of hydroxamates, particularly with respect to CNS-penetration, distribution, and retention. To explore the rodent and non-human primate (NHP) brain permeability of hydroxamic acid-based HDAC inhibitors using positron emission tomography (PET), we modified the structures of belinostat (PXD101) and panobinostat (LBH-589) to incorporate carbon-11. We also labeled PCI 34051 through carbon isotope substitution. After characterizing the *in vitro* affinity and efficacy of these compounds across nine recombinant HDAC isoforms spanning Class I and Class II family members, we determined the brain uptake of each inhibitor. Each labeled compound has low uptake in brain tissue when administered intravenously to rodents and NHPs. In rodent studies, we observed that brain accumulation of the radiotracers were unaffected by the pre-administration of unlabeled inhibitors. Knowing that CNS-penetration may be desirable for both imaging applications and therapy, we explored whether a liquid chromatography, tandem mass spectrometry (LC-MS-MS) method to predict brain penetrance would be an appropriate method to pre-screen compounds (hydroxamic acid-based HDACi) prior to PET radiolabeling. LC-MS-MS data were indeed useful in identifying additional lead molecules to explore as PET imaging agents to visualize HDAC enzymes *in vivo*. However, HDACi brain penetrance predicted by LC-MS-MS did not strongly correlate with PET imaging results. This underscores the importance of *in vivo* PET imaging tools in characterizing putative CNS drug lead compounds and the continued need to discover effect PET tracers for neuroepigenetic imaging.

Keywords: Hydroxamic acid, HDAC inhibitors, epigenetic, PET, brain, imaging

Introduction

Histone proteins and their associated DNA together comprise nucleosomes, the fundamental unit of chromatin structure and the structural base for DNA condensation. Covalent chemical modification of histones via processes such as acetylation, methylation, ubiquitination and phosphorylation [1], play a critical role

in the dynamic regulation of gene expression through chromatin remodeling and modulating transcription factor binding.

Histone acetylation is regulated by the opposing actions of two enzyme classes, histone acetyltransferases (HATs) and histone deacetylases (HDACs) [2-4]. HDAC enzymes are divided into four different classes based on sequence

HDAC imaging

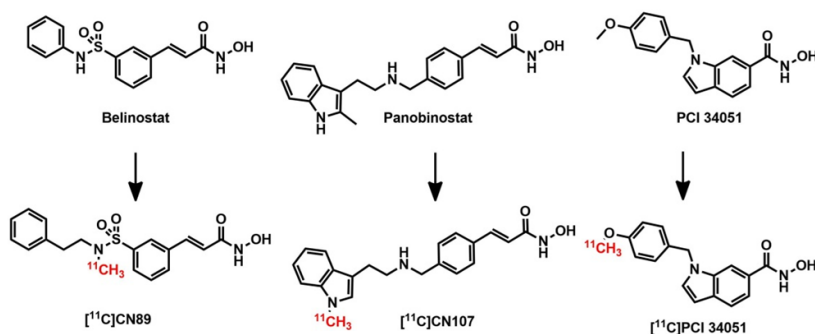


Figure 1. Structures of selected HDAC inhibitors on clinical trials and the potential PET radiotracers derived from these HDACis.

homology, cellular localization and phylogenetic relationships to yeast homologues [5]: class I (HDACs 1, 3, 8), class IIa (HDACs 4, 5, 7, 9), class IIb (HDACs 6, 10), class III (SIRT1, 7), and class IV (HDAC 11). Classes I, II and IV are zinc dependent enzymes. Increases in histone acetylation causes relaxation of higher order chromatin structure and contributes to activation of gene expression [6]. Importantly, histone acetylation-mediated changes in gene expression are cell-type specific and outcomes range from necrosis, cytostasis, and apoptosis in cancerous cells to robust neuronal differentiation in neural precursors and enhancement of synaptogenesis [7, 8]. As such, deficiencies in histone acetylation and transcriptional dysfunction have been implicated in cancer pathology as well as in a number of neurodegenerative diseases including Huntington's [9-12], Parkinson's and Alzheimer's diseases [9, 13-15], amyotrophic lateral sclerosis [16, 17], spinal muscular atrophy [18] and stroke [13-15]. Clarifying the role of HDAC function in normal and disease biology has direct relevance to therapeutic development [19, 20].

HDAC inhibitors (HDACis) have emerged as promising drug candidates to restore the balance of HDAC and histone acetyl-transferase (HAT) enzymes in disease. Class I, II and IV HDAC enzymes are zinc dependent and can be inhibited by compounds with zinc-chelating moieties. These compounds comprise diverse structural classes [21-27] including the most widely-investigated, the hydroxamic acids [22]. Following the initial discovery that the hydroxamic acid, trichostatin A, was a strong inhibitor of HDAC targets ($K_i = 3.4$ nM) [28], research led to the development of suberoyl-anilide hydroxamic acid (SAHA, vorinostat) which was FDA-approved for the treatment of

cutaneous T-cell lymphomas (CTCL). This provided key evidence that HDAC inhibitors, including those hydroxamic acid-based structures, could have therapeutic potential.

Thus, cinnamic acid derivatives have been intensely investigated as HDAC inhibitors. Several compounds from this class have advanced into clinical

trials, including belinostat and panobinostat. Belinostat is a potent HDACi ($IC_{50} = 27$ nM), with the sulfonamide substitute in the *meta* position, and is undergoing phase II trials in solid tumors (ovarian, hepatocarcinoma, mesothelioma) [29]. Panobinostat, an almost equally potent HDACi ($IC_{50} = 37$ nM), is currently in phase II/III clinical trials for chronic myeloid leukemia, refractory CTCL, and multiple myeloma [30]. In addition to cinnamic acids, the phenyl hydroxamate, PCI 34051 is the most subtype selective HDAC inhibitor identified to date. This compound has a reported $IC_{50} = 10$ nM for HDAC8 - revealing greater than 100-fold selectivity over other HDAC subtypes [31]. Selective HDAC inhibition is increasingly used to clarify understanding of the biological role of HDAC subtypes [32, 33]. However, PCI 34051 remains underutilized as a highly selective HDAC inhibitor and could provide insight into the role of HDAC8. Despite their potential as therapeutic leads and tool compounds, little is known about how these three inhibitors impact HDAC targets in the living brain.

LC-MS-MS can be used to measure the brain penetration of a compound, although is invasive, requiring brain removal thereby limiting its application to pre-clinical models. Developing an imaging tool that permits detection and quantification of HDAC expression *in vivo* is critical to assess the efficacy of HDAC-targeted therapies and to clarify the understanding of the mechanism of HDAC enzyme dysfunction in disease. Positron emission tomography (PET) is an excellent tool for the *in vivo* quantification of HDAC biological processes as well as evaluation of the pattern of HDAC distribution in animals and human. A few fluorine-18 labeled compounds ($[^{18}\text{F}]\text{FAHA}$ [34], $[^{18}\text{F}]\text{SAHA}$ [35]) have been reported and demonstrate the

HDAC imaging

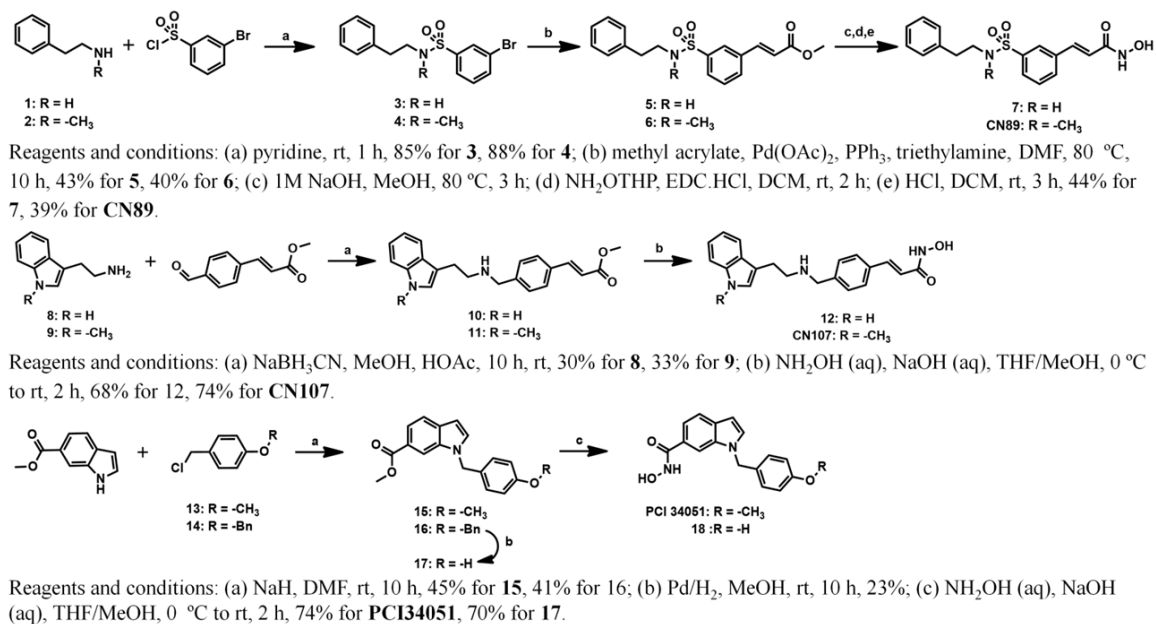


Figure 2. Synthesis of HDAC inhibitors and their precursors for carbon-11 labeling.

potential for *in vivo* HDAC imaging in animals, although to date, no *in vivo* imaging studies have evaluated the brain penetrance of hydroxamic acid-based HDACi [36]. Rodent studies have shown that the BBB penetrance of SAHA is very low, but as a class, the brain availability hydroxamic acids is largely unexplored [37].

In our experiments, we utilized *in vivo* PET imaging in rodent and non-human primate to characterize blood-brain barrier (BBB) penetration [38, 39] of select carbon-11 labeled hydroxamic acid-based HDAC inhibitors. We additionally compared BBB penetrance predicted by LC-MS-MS methods. The results of our findings are presented and discussed below.

Results

Chemical synthesis

To incorporate carbon-11, we modified the structures of belinostat and panobinostat, as shown in **Figure 1**. **PCI34051** has a methoxyl group and thus could be labeled without structural modification. The synthesis of the HDAC inhibitors and their carbon-11 labeling precursors are shown in **Figure 2**. Briefly, *N*-methyl-2-phenylethanamine was reacted with 3-bromobenzene-1-sulfonyl chloride to form intermediate **4**, which was then coupled with methyl

acrylate catalyzed by Pd(OAc)₂ to provide the methyl ester **6**. Methyl ester **6** was hydrolyzed with 1 M NaOH, then coupled with NH₂-OHP, and converted to the target hydroxamate **CN89** after deprotection of THP in the presence of HCl. The synthesis of precursor **7** was synthesized by a similar route, starting from phenylethanamine. Reductive amination of 4-formylcinnamic methyl ester with a primary amines afforded methyl esters **10** and **11**. Methyl esters were treated with hydroxylamine (hydroxylamine, excessive sodium methoxide in methanol/THF) and converted to the target hydroxamates, **CN107** and its precursor **12**. Methyl 1*H*-indole-6-carboxylate was reacted with **13** or **14** in the presence of sodium hydride to afford intermediate **15** or **16**. Methyl ester **15** was treated with hydroxylamine to obtain **PCI 34051**. Its precursor **18** was achieved by hydrogenation, followed by treatment with hydroxylamine.

In vitro HDAC assay

The *in vitro* inhibitory activities of **CN89**, **CN107**, and **PCI 34051** were measured for each HDAC isoform HDAC1 through HDAC9 (**Table 1**). The IC₅₀ value for SAHA was measured in parallel as a reference. The synthesized belinostat analog **CN 89** showed low nanomolar IC₅₀ towards class-I HDAC isoforms (HDAC1-3) as well as toward class-II HDAC isoform (HDAC6). The pan-

Table 1. HDAC isoforms selectivity data for selected HDAC inhibitors

| Compound | IC ₅₀ [nM] | | | | | | | | |
|-----------|-----------------------|-------|-------|-------|-------|-------|-------|-------|-------|
| | HDAC1 | HDAC2 | HDAC3 | HDAC4 | HDAC5 | HDAC6 | HDAC7 | HDAC8 | HDAC9 |
| SAHA | 4 | 11 | 3 | 40200 | 8750 | 2.2 | 42800 | 1020 | 70000 |
| CN89 | 5 | 32 | 3.4 | 500 | 10732 | 5 | 44488 | 150 | 16904 |
| CN107 | 0.19 | 1.15 | 0.38 | 655 | 99 | 1.6 | 2044 | 1044 | 4849 |
| PCI 34051 | 36400 | 1740 | 50300 | - | 70000 | 7390 | 70000 | 18.3 | 70000 |

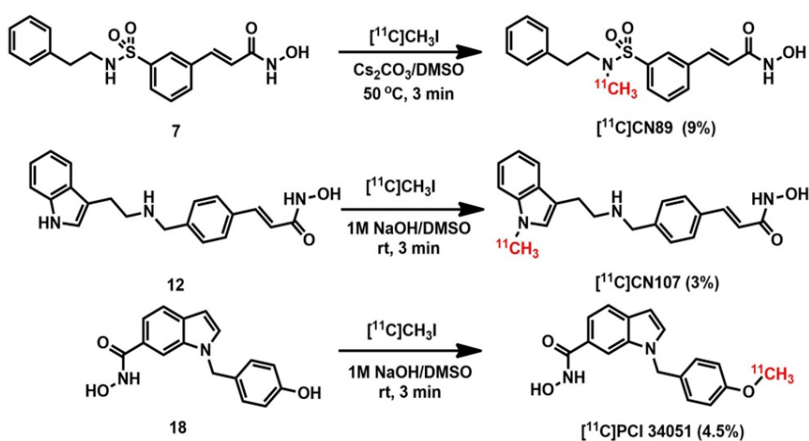


Figure 3. Radiosynthesis of [¹¹C]CN89 (RCY: 9%, non-decay corrected to trapped [¹¹C]CH₃I with a specific activity 0.8±0.2 Ci/μmol (EOB)); [¹¹C]CN107 (RCY: 3%, non-decay corrected to trapped [¹¹C]CH₃I with a specific activity 0.9±0.1 Ci/μmol (EOB)); and [¹¹C]PCI 34051 (RCY: 4.5%, non-decay corrected to trapped [¹¹C]CH₃I with a specific activity 0.7±0.2 Ci/μmol (EOB)).

obinostat derivative, **CN107**, also showed low nanomolar IC₅₀ towards the same class-I HDAC isoforms, indicating that the methyl group we introduced did not significantly degrade the affinity or selectivity of these compounds. The IC₅₀ value of **PCI 34051** for HDAC8, using an activity assay different than that previously described [40, 41], was found to be 18.2 nM, which is greater than 100-fold selectivity over each of the other HDAC isoforms.

Radiosynthesis of selected HDAC inhibitors

The synthesis of the candidate radiotracers was accomplished using precursors in DMSO with [¹¹C]methyl iodine ([¹¹C]CH₃I) as outlined in **Figure 3**. ¹¹CH₃I was trapped in a TRACERlab FX-M synthesizer reactor preloaded with a solution of precursor **7** (1.0 mg) and Cs₂CO₃ (6.0 mg) for **CN89**; precursor **12** (1.0 mg) and 10 μl of 1 M NaOH for **CN107**; precursor **18** (1.0 mg) and 10 μl of 1 M NaOH for **PCI 34051** in dry DMSO (300 μL). The solution was stirred under pressure at 50 °C (**CN89**) or room temp (**CN107** and **PCI 34051**) for 3 min and then water (1.2

mL) was added. The reaction mixture was purified by reverse phase semi-preparative HPLC and the desired fraction was collected. The final product was reformulated by loading water-diluted eluent onto a solid-phase exchange (SPE) C-18 cartridge. The SPE was rinsed with H₂O (5 mL) and the isolated material was eluted from the SPE with EtOH (1 mL followed by saline (0.9%, 9 mL). The chemical and radiochemical purity of the final product was determined by analytical HPLC.

The identity of the product was confirmed by analytical HPLC by co-elution comparison to a reference standard. The average time required for the synthesis from end of cyclotron bombardment to end of synthesis was 34 min (**CN89**), 37 min (**CN107**) and 36 min (**PCI 34051**). The radiochemical yield was 9% (**CN89**), 3% (**CN107**) and 4.5% (**PCI 34051**) (non-decay corrected relative to trapped [¹¹C]CH₃I). Chemical and radiochemical purities were ≥ 95% for all radiotracers.

PET imaging in rodents and NHPs

Using PET-CT, we determined that all labeled compounds exhibited very poor initial BBB penetration and low brain uptake over the scanning time (60 min) when administered intravenously to rats (0.9-1.1 mCi per scan), as shown in **Figure 4**. A concentration of less than 0.15 %ID/cc was distributed in the brain tissue after administration of [¹¹C]CN89 and [¹¹C]CN107. We also conducted the PET imaging study with the pretreatment of reference standards (2

HDAC imaging

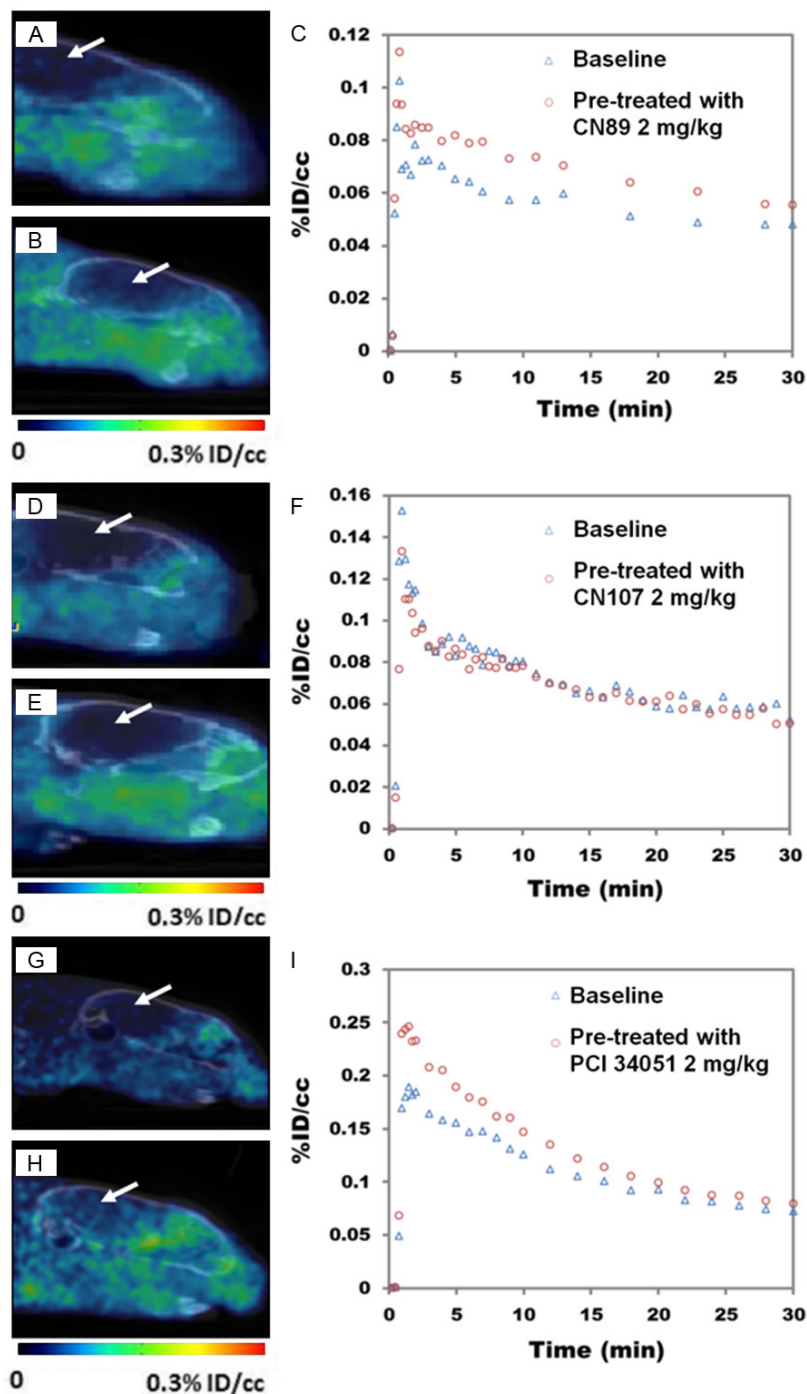


Figure 4. Rodent imaging experiments with radiotracers. Summed PET images (1-60 min) following injection of $[^{11}\text{C}]\text{CN89}$ (A), $[^{11}\text{C}]\text{CN107}$ (D) and $[^{11}\text{C}]\text{PCI 34051}$ (G) baseline scans; summed PET-CT images (1-60 min) images acquired following pretreatment with corresponding unlabeled inhibitors (B: **CN89**; E: **CN107**; H: **PCI 34051**) (2 mg/kg, iv). Images are dose corrected. Whole-brain time-activity curves generated from rodents PET imaging data (0-30 min) for $[^{11}\text{C}]\text{CN89}$ (C), $[^{11}\text{C}]\text{CN107}$ (F) and $[^{11}\text{C}]\text{PCI 34051}$ (I).

mg/kg); however, we did not observe a change in permeability or retention after pretreatment.

To further investigate the brain permeability of the carbon-11 labeled compounds, we conducted imaging in *Papio anubis* baboons. Using PET-MRI, we further determined that $[^{11}\text{C}]\text{CN89}$, $[^{11}\text{C}]\text{CN107}$ and $[^{11}\text{C}]\text{PCI 34051}$ exhibited very poor BBB penetration and low brain uptake over the scanning time (80 min) when the radiotracers (4-5 mCi) were administered intravenously, **Figure 5**. Coregistration of the PET image with an MRI of the same animal indicated that some radioactivity indeed partitioned into brain tissue, albeit at low levels.

Brain uptake test with LC-MS-MS method

According to the LC-MS-MS results, **CN89** showed higher standardized uptake values (SUV) and brain to plasma ratio than **CN107** and **PCI 34051**, which showed low uptake in the brain; as a subsequent LC-MS-MS screen, we chose three additional compounds (**19**, **20** and **21**) (IC_{50} : **19**: HDAC1 = 19.2 nM, HDAC2 = 109 nM, HDAC3 = 79.3 nM; **20**: HDAC1 = 165 nM, HDAC2 = 660 nM, HDAC3 = 90 nM; **21**: HDAC1 = 56.1 nM, HDAC2 = 53.7 nM, HDAC3 = 7.1 nM) to evaluate for brain uptake. We chose these compounds based on their hydroxamic acid structure. Compounds **19** and **20** showed low SUV (0-4% in hippocampus, **Table 2**) indicating they are likely not brain penetrant.

Compound **21** showed high SUV (in hippocampus) and brain (hippocampus) to plasma ratio

HDAC imaging

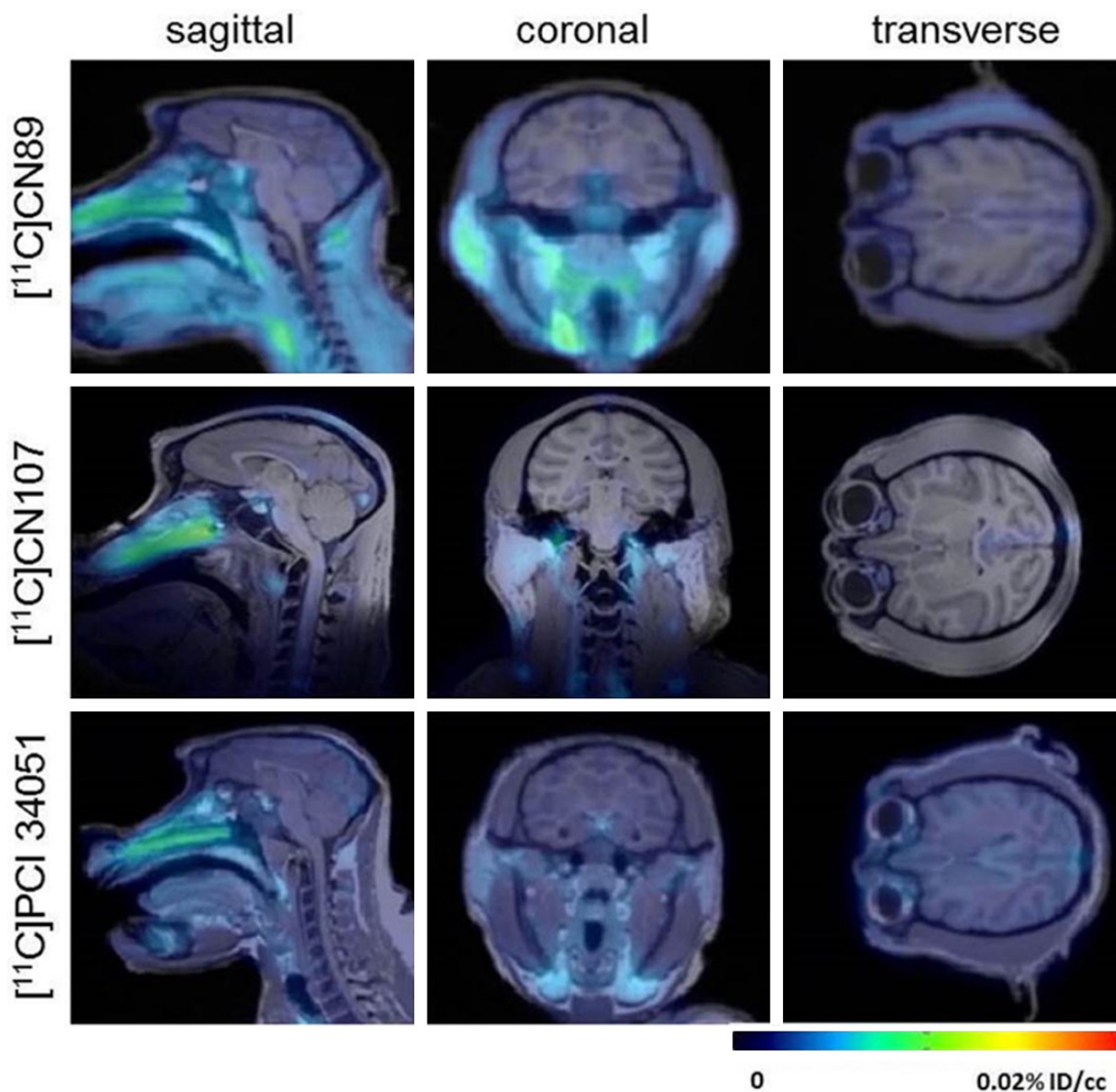


Figure 5. PET-MRI Imaging (baboon brain). Summed PET images (0-80 min) superimposed with a MEMPRAGE-MRI of the brain from the same baboon, following injection of radiotracers (4-5 mCi/baboon). Top row: $[^{11}\text{C}]\text{CN89}$; middle row: $[^{11}\text{C}]\text{CN107}$; bottom row: $[^{11}\text{C}]\text{PCI 34051}$.

(Table 2) indicating CNS penetrance of this compound.

Discussion

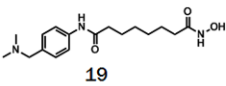
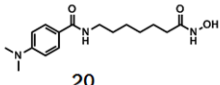
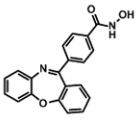
HDACs play an important role in diseases, including, but not limited to, brain disorders, heart disease and cancers, but there is no method to measure the HDAC expression in human with such diseases and monitor the disease progress and evaluate the therapeutics. To measure and quantification of HDAC expression non-invasive *in vivo*, PET would be an ideal tool, however, there is still no validated PET radiotracer available for HDAC imaging, particu-

larly in the brain. We chose some HDAC inhibitors, current in the clinical trials, to incorporate the positron emission isotopes to test the brain permeability of these inhibitors. After structural modifications, the compounds are easy to incorporate with carbon-11 and remain the high binding towards HDACs.

To evaluate their brain permeability, we conduct PET imaging with rodents and NHPs. The summed PET-CT images showed that the radioactivity within the skull from all the three tracers is likely outside of the BBB and represents the blood pool within the rats brain (Figure 4). The NHP imaging results were consistent with

HDAC imaging

Table 2. Physicochemical properties of selected hydroxamic acid HDAC inhibitors and the evaluation of CNS permeability with LC-MS-MS

| Compound | Molecular Weight | Log P | tPSA | %SUV @20 min | B/P @20 min |
|--|------------------|-------|-------|--------------|-------------|
|  19 | 321.41 | 1.74 | 81.67 | 0 | 0 |
|  20 | 307.39 | 2.07 | 81.67 | 4 | 0.36 |
| CN107 | 349.43 | 2.66 | 64.6 | 8 | 1 |
| PCI 34051 | 296.32 | 2.61 | 61.8 | 30 | 0 |
| CN89 | 360.43 | 2.03 | 86.71 | 77 | 6 |
|  21 | 330.34 | 3.64 | 70.92 | 222 | 4.5 |

SUV = Standardized Uptake Volume (% Tracer conc. in Hippocampus @20 min). B/P = Brain to Plasma ratio (Hippocampus/Plasma).

the PET experiments we conducted in rodents, showing the limited brain uptake with these radiolabeled compounds. Additional experiments will be needed both *in vitro* and *in vivo* to determine the reason these hydroxamic acid HDACis have poor CNS permeability.

Given that PET imaging is a relatively slow and costly means of 'screening' HDAC imaging candidates, we additionally utilized LC-MS-MS as an established and low-cost method to identify lead molecules with good BBB penetration and specific binding (at microdoses). LC-MS-MS has been used for the assessment of brain tracer distribution of dopamine D2, serotonin 2A and NK-1 receptors [42]. Using these published methods, our LC-MS-MS results indicated that **CN89** showed higher standardized uptake values (SUV) and brain to plasma ratio than **CN107** and **PCI 34051**; however, via *in vivo* PET imaging, [^{14}C]**PCI 34051** had the highest %ID/cc compared to [^{14}C]**CN89** and [^{14}C]**CN107**. One possibility why the PET and LC-MS-MS data were not consistent is that the injected mass of unlabeled compounds for LC-MS-MS detection is at least 10-fold larger (in 2-3 microgram range) compared with nanogram amounts for PET imaging (200-300 nanograms). Thus, the BBB may only effectively prevent a small amount (nanograms) of compound from reaching the brain, resulting in a lack of CNS tracer uptake as visualized by PET. Experiments to test this directly are not feasible as it is not ethical to deliver microgram quantities of radiolabeled compound for *in vivo* PET imaging nor is

it possible to detect nanogram amounts of compound using current LC-MS-MS methods. Additional screening of HDACis with LC-MS-MS method indicates that compound **21** has potential to be used as new CNS radiotracers and HDAC inhibitors.

Overall, these results still indicate that LC-MS-MS could be used as a preliminary screening tool for the CNS radiotracer development as, compared to PET imaging, it is a low-cost and high-throughput technique. However PET imaging provides a unique advantage as a non-invasive technique that can provide a visual representation of a labeled compound in a living brain.

Conclusions

In summary, we successfully synthesized and characterized binding affinity for [^{14}C]hydroxamic acid-based HDAC inhibitors **CN89**, **CN107**, and **PCI 34051**. PET studies performed in conjunction with CT and MRI evaluated the brain uptake of these radiotracers, demonstrating poor BBB penetration in rats as well as in baboon. Our PET imaging data indicate these compounds are not effective tracers for diseases localized in the CNS. However our experiments have not ruled out the potential utility of these candidate probes for imaging and therapy in non-CNS diseases, such as peripheral cancers. The development of CNS-penetrant HDAC imaging probes and the evaluation of [^{14}C]**CN89**, [^{14}C]**CN107** and [^{14}C]**PCI 34051** as

peripheral PET imaging probes are currently underway.

Supporting information

The section discussing materials and methods is included in SI. This section describes chemical synthesis, radiolabeling used in this study. Assay procedures for determination of *in vitro* enzymatic assay for histone deacetylases, LC-MS-MS method and animal imaging experiments are also detailed in SI.

Acknowledgements

The project described was supported by Award Number 1R01DA030321 and 1R01DA028301 from the National Institutes of Health (NIH) and this research was carried out at the Athinoula A. Martinos Center for Biomedical Imaging at the Massachusetts General Hospital, using resources provided by the Center for Functional Neuroimaging Technologies, P41EB015896, a P41 Regional Resource supported by the National Institute of Biomedical Imaging and Bioengineering (NIBIB), National Institutes of Health. This work also involved the use of instrumentation supported by the NIH Shared Instrumentation Grant Program and/or High-End Instrumentation Grant Program; specifically, grant numbers: S10RR017208, S10RR026666, S10RR022976, S10RR019933, S10RR029495. We would like to thank members of the Martinos Center PET Production and Imaging facility for assistance with radiochemistry and imaging: Colin Wilson, Chris Moseley, Steve Carlin, Shirley Hsu and Grae Arabasz. The authors are also grateful to Joseph Mandeville and Helen Deng for assistance during NHP imaging.

Disclosure of conflict of interest

None.

Address correspondence to: Dr. Jacob M Hooker, Athinoula A. Martinos Center for Biomedical Imaging, Department of Radiology, Massachusetts General Hospital, Harvard Medical School, 149 13th Street Suite 2301, Charlestown, MA 02129, USA. Tel: 617-726-6596; Fax: 617-726-7422; E-mail: hooker@nmr.mgh.harvard.edu

References

[1] Yoo CB and Jones PA. Epigenetic therapy of cancer: past, present and future. *Nat Rev Drug Discov* 2006; 5: 37-50.

[2] Mai A, Massa S, Rotili D, Cerbara I, Valente S, Pezzi R, Simeoni S and Ragno R. Histone deacetylation in epigenetics: an attractive target for anticancer therapy. *Med Res Rev* 2005; 25: 261-309.

[3] Langley B, Gensert JM, Beal MF and Ratan RR. Remodeling chromatin and stress resistance in the central nervous system: histone deacetylase inhibitors as novel and broadly effective neuroprotective agents. *Curr Drug Targets CNS Neurol Disord* 2005; 4: 41-50.

[4] Abel T and Zukin RS. Epigenetic targets of HDAC inhibition in neurodegenerative and psychiatric disorders. *Curr Opin Pharmacol* 2008; 8: 57-64.

[5] de Ruijter AJ, van Gennip AH, Caron HN, Kemp S and van Kuilenburg AB. Histone deacetylases (HDACs): characterization of the classical HDAC family. *Biochem J* 2003; 370: 737-749.

[6] Bolden JE, Peart MJ and Johnstone RW. Anti-cancer activities of histone deacetylase inhibitors. *Nat Rev Drug Discov* 2006; 5: 769-784.

[7] Shi P, Scott MA, Ghosh B, Wan D, Wissner-Gross Z, Mazitschek R, Haggarty SJ and Yanik MF. Synapse microarray identification of small molecules that enhance synaptogenesis. *Nat Commun* 2011; 2: 510.

[8] Fass DM, Reis SA, Ghosh B, Hennig KM, Joseph NF, Zhao WN, Nieland TJ, Guan JS, Kuhnle CE, Tang W, Barker DD, Mazitschek R, Schreiber SL, Tsai LH and Haggarty SJ. Crebinostat: a novel cognitive enhancer that inhibits histone deacetylase activity and modulates chromatin-mediated neuroplasticity. *Neuropharmacology* 2013; 64: 81-96.

[9] Steffan JS, Bodai L, Pallos J, Poelman M, McCampbell A, Apostol BL, Kazantsev A, Schmidt E, Zhu YZ, Greenwald M, Kurokawa R, Housman DE, Jackson GR, Marsh JL and Thompson LM. Histone deacetylase inhibitors arrest polyglutamine-dependent neurodegeneration in *Drosophila*. *Nature* 2001; 413: 739-743.

[10] Bates EA, Victor M, Jones AK, Shi Y and Hart AC. Differential contributions of *Caenorhabditis elegans* histone deacetylases to huntingtin polyglutamine toxicity. *J Neurosci* 2006; 26: 2830-2838.

[11] Pallos J, Bodai L, Lukacsovich T, Purcell JM, Steffan JS, Thompson LM and Marsh JL. Inhibition of specific HDACs and sirtuins suppresses pathogenesis in a *Drosophila* model of Huntington's disease. *Hum Mol Genet* 2008; 17: 3767-3775.

[12] Graff J, Rei D, Guan JS, Wang WY, Seo J, Hennig KM, Nieland TJ, Fass DM, Kao PF, Kahn M, Su SC, Samiei A, Joseph N, Haggarty SJ, Delalle I and Tsai LH. An epigenetic blockade of cognitive functions in the neurodegenerating brain. *Nature* 2012; 483: 222-226.

HDAC imaging

- [13] Ren M, Leng Y, Jeong M, Leeds PR and Chuang DM. Valproic acid reduces brain damage induced by transient focal cerebral ischemia in rats: potential roles of histone deacetylase inhibition and heat shock protein induction. *J Neurochem* 2004; 89: 1358-1367.
- [14] Kim HJ, Rowe M, Ren M, Hong JS, Chen PS and Chuang DM. Histone deacetylase inhibitors exhibit anti-inflammatory and neuroprotective effects in a rat permanent ischemic model of stroke: multiple mechanisms of action. *J Pharmacol Exp Ther* 2007; 321: 892-901.
- [15] Faraco G, Pancani T, Formentini L, Mascagni P, Fossati G, Leoni F, Moroni F and Chiarugi A. Pharmacological inhibition of histone deacetylases by suberoylanilide hydroxamic acid specifically alters gene expression and reduces ischemic injury in the mouse brain. *Mol Pharmacol* 2006; 70: 1876-1884.
- [16] Ryu H, Smith K, Camelo SI, Carreras I, Lee J, Iglesias AH, Dangond F, Cormier KA, Cudkowicz ME, Brown RH Jr and Ferrante RJ. Sodium phenylbutyrate prolongs survival and regulates expression of anti-apoptotic genes in transgenic amyotrophic lateral sclerosis mice. *J Neurochem* 2005; 93: 1087-1098.
- [17] Del Signore SJ, Amante DJ, Kim J, Stack EC, Goodrich S, Cormier K, Smith K, Cudkowicz ME and Ferrante RJ. Combined riluzole and sodium phenylbutyrate therapy in transgenic amyotrophic lateral sclerosis mice. *Amyotroph Lateral Scler* 2009; 10: 85-94.
- [18] Cudkowicz ME, Andres PL, Macdonald SA, Bedlack RS, Choudry R, Brown RH Jr, Zhang H, Schoenfeld DA, Shefner J, Matson S, Matson WR and Ferrante RJ. Phase 2 study of sodium phenylbutyrate in ALS. *Amyotroph Lateral Scler* 2009; 10: 99-106.
- [19] Schroeder FA, Lewis MC, Fass DM, Wagner FF, Zhang YL, Hennig KM, Gale J, Zhao WN, Reis S, Barker DD, Berry-Scott E, Kim SW, Clore EL, Hooker JM, Holson EB, Haggarty SJ and Petryshen TL. A Selective HDAC 1/2 Inhibitor Modulates Chromatin and Gene Expression in Brain and Alters Mouse Behavior in Two Mood-Related Tests. *PLoS One* 2013; 8: e71323.
- [20] Schroeder FA, Chonde DB, Riley MM, Moseley CK, Granda ML, Wilson CM, Wagner FF, Zhang YL, Gale J, Holson EB, Haggarty SJ and Hooker JM. FDG-PET imaging reveals local brain glucose utilization is altered by class I histone deacetylase inhibitors. *Neurosci Lett* 2013; 550: 119-124.
- [21] Phiel CJ, Zhang F, Huang EY, Guenther MG, Lazar MA and Klein PS. Histone deacetylase is a direct target of valproic acid, a potent anticonvulsant, mood stabilizer, and teratogen. *J Biol Chem* 2001; 276: 36734-36741.
- [22] Marks PA and Breslow R. Dimethyl sulfoxide to vorinostat: development of this histone deacetylase inhibitor as an anticancer drug. *Nat Biotechnol* 2007; 25: 84-90.
- [23] Ueda H, Manda T, Matsumoto S, Mukumoto S, Nishigaki F, Kawamura I and Shimomura K. FR901228, a novel antitumor bicyclic depsipeptide produced by *Chromobacterium violaceum* No. 968. III. Antitumor activities on experimental tumors in mice. *J Antibiot (Tokyo)* 1994; 47: 315-323.
- [24] Berger MR, Bischoff H, Fritschi E, Henne T, Herrmann M, Pool BL, Satzing G, Schmahl D and Weiershausen U. Synthesis, toxicity, and therapeutic efficacy of 4-amino-N-(2'-aminophenyl)benzamide: a new compound preferentially active in slowly growing tumors. *Cancer Treat Rep* 1985; 69: 1415-1424.
- [25] Kraker AJ, Mizzen CA, Hartl BG, Miin J, Allis CD and Merriman RL. Modulation of histone acetylation by [4-(acetylamino)-N-(2-amino-phenyl) benzamide] in HCT-8 colon carcinoma. *Mol Cancer Ther* 2003; 2: 401-408.
- [26] Frey RR, Wada CK, Garland RB, Curtin ML, Michaelides MR, Li J, Pease LJ, Glaser KB, Marcotte PA, Bouska JJ, Murphy SS and Davidsen SK. Trifluoromethyl ketones as inhibitors of histone deacetylase. *Bioorg Med Chem Lett* 2002; 12: 3443-3447.
- [27] Vasudevan A, Ji Z, Frey RR, Wada CK, Steinman D, Heyman HR, Guo Y, Curtin ML, Guo J, Li J, Pease L, Glaser KB, Marcotte PA, Bouska JJ, Davidsen SK and Michaelides MR. Heterocyclic ketones as inhibitors of histone deacetylase. *Bioorg Med Chem Lett* 2003; 13: 3909-3913.
- [28] Vanhaecke T, Papeleu P, Elaut G and Rogiers V. Trichostatin A-like hydroxamate histone deacetylase inhibitors as therapeutic agents: toxicological point of view. *Curr Med Chem* 2004; 11: 1629-1643.
- [29] Plumb JA, Finn PW, Williams RJ, Bandara MJ, Romero MR, Watkins CJ, La Thangue NB and Brown R. Pharmacodynamic response and inhibition of growth of human tumor xenografts by the novel histone deacetylase inhibitor PXD101. *Mol Cancer Ther* 2003; 2: 721-728.
- [30] Giles F, Fischer T, Cortes J, Garcia-Manero G, Beck J, Ravandi F, Masson E, Rae P, Laird G, Sharma S, Kantarjian H, Dugan M, Albitar M and Bhalla K. A phase I study of intravenous LBH589, a novel cinnamic hydroxamic acid analogue histone deacetylase inhibitor, in patients with refractory hematologic malignancies. *Clin Cancer Res* 2006; 12: 4628-4635.
- [31] Balasubramanian S, Ramos J, Luo W, Sirisawad M, Verner E and Buggy JJ. A novel histone deacetylase 8 (HDAC8)-specific inhibitor PCI-34051 induces apoptosis in T-cell lymphomas. *Leukemia* 2008; 22: 1026-1034.
- [32] Espallergues J, Teegarden SL, Veerakumar A, Boulden J, Challis C, Jochems J, Chan M, Pe-

HDAC imaging

- tersen T, Deneris E, Matthias P, Hahn CG, Lucki I, Beck SG and Berton O. HDAC6 regulates glucocorticoid receptor signaling in serotonin pathways with critical impact on stress resilience. *J Neurosci* 2012; 32: 4400-4416.
- [33] Malvaez M, McQuown SC, Rogge GA, Astarabadi M, Jacques V, Carreiro S, Rusche JR and Wood MA. HDAC3-selective inhibitor enhances extinction of cocaine-seeking behavior in a persistent manner. *Proc Natl Acad Sci U S A* 2013; 110: 2647-2652.
- [34] Yeh HH, Tian M, Hinz R, Young D, Shavrin A, Mukhopadhyay U, Flores LG, Balatoni J, Soghomonyan S, Jeong HJ, Pal A, Uthamanthil R, Jackson JN, Nishii R, Mizuma H, Onoe H, Kagawa S, Higashi T, Fukumitsu N, Alauddin M, Tong W, Herholz K and Gelovani JG. Imaging epigenetic regulation by histone deacetylases in the brain using PET/MRI with (1)(8)F-FAHA. *Neuroimage* 2013; 64: 630-639.
- [35] Hendricks JA, Keliher EJ, Marinelli B, Reiner T, Weissleder R and Mazitschek R. In vivo PET imaging of histone deacetylases by 18F-suberoyl-anilide hydroxamic acid (18F-SAHA). *J Med Chem* 2011; 54: 5576-5582.
- [36] Wang Y, Zhang YL, Hennig K, Gale JP, Hong Y, Cha A, Riley M, Wagner F, Haggarty SJ, Holson E and Hooker J. Class I HDAC imaging using [(3)H]CI-994 autoradiography. *Epigenetics* 2013; 8: 756-64.
- [37] Hanson JE, La H, Plise E, Chen YH, Ding X, Hania T, Sabath EV, Alexandrov V, Brunner D, Leahy E, Steiner P, Liu L, Scarce-Levie K and Zhou Q. SAHA Enhances Synaptic Function and Plasticity In Vitro but Has Limited Brain Availability In Vivo and Does Not Impact Cognition. *PLoS One* 2013; 8: e69964.
- [38] Hooker JM, Kim SW, Alexoff D, Xu Y, Shea C, Reid A, Volkow N and Fowler JS. Histone deacetylase inhibitor, MS-275, exhibits poor brain penetration: PK studies of [C]MS-275 using Positron Emission Tomography. *ACS Chem Neurosci* 2010; 1: 65-73.
- [39] Kim SW, Hooker JM, Otto N, Win K, Muench L, Shea C, Carter P, King P, Reid AE, Volkow ND and Fowler JS. Whole-body pharmacokinetics of HDAC inhibitor drugs, butyric acid, valproic acid and 4-phenylbutyric acid measured with carbon-11 labeled analogs by PET. *Nucl Med Biol* 2013; 40: 912-8.
- [40] Wagner FF, Olson DE, Gale JP, Kaya T, Weiwer M, Aidoud N, Thomas M, Davoine EL, Lemercier BC, Zhang YL and Holson EB. Potent and selective inhibition of histone deacetylase 6 (HDAC6) does not require a surface-binding motif. *J Med Chem* 2013; 56: 1772-1776.
- [41] Holson E, Wagner FF, WeiWwer M, Tsai LH, Haggarty S, Zhang YL. Inhibitors Of Histone Deacetylase. WO2012149540 2012.
- [42] Chernet E, Martin LJ, Li D, Need AB, Barth VN, Rash KS and Phebus LA. Use of LC/MS to assess brain tracer distribution in preclinical, in vivo receptor occupancy studies: dopamine D2, serotonin 2A and NK-1 receptors as examples. *Life Sci* 2005; 78: 340-346.